A weakly nonlinear model for sound propagation in brass instruments

Freddie Jensen[1]
Warwick Maths Institute,
University of Warwick, Coventry, CV4 7AL, UK.

Edward James Brambley[2]
Warwick Maths Institute and WMG,
University of Warwick, Coventry, CV4 7AL, UK.

ABSTRACT

We present a summary of work on a new weakly nonlinear model of sound in curved 2D or 3D waveguides without mean flow. The duct geometry allows for curvature and width variation, and also in 3D for torsion. Equations are projected onto a Frenet-Serret frame with arclength s, then expanded at each s in terms of the modes of an equiradial straight duct. This is the multi-modal method. We introduce a matricial admittance that encodes the radiative properties of the duct; this allows for the prescription of a radiation condition at the duct outlet. Previous modelling has taken this to be the characteristic admittance: while mathematically tractable, this is highly physically idealised and corresponds to a duct opening into a room of equal radius. We instead derive a radiation condition consisting of a greatly enlarged duct with the original duct at the centre, which tells us more about the passage of sound from the outlet. This allows for more direct physical comparisons with the model, e.g. the end correction for organ pipes or the harmonic series of a trumpet.

1. INTRODUCTION

It has been experimentally established, in Hirschberg et al. [1] among other papers, that shock waves can form in brass instruments. From this the deduction has been made that shock waves are a contributing factor to the distinctive 'brassiness' of the sound that they make. Much of the modelling of this problem has simplified the physics by examining wave propagation in straight waveguides (albeit in some cases with width variation [e.g. 2]). The geometry of the brass instruments used in the vast majority of modern performance contexts exhibits greater complexity than this, not only due to the use of valves, but also due to curvature and torsion (these being necessary for the practicalities of achieving long waveguides in a confined space). Work on the latter problem, i.e. propagation in curved waveguides, has largely taken place in a linear acoustic regime [e.g. 3], in which shock waves cannot occur. McTavish and Brambley [4] attempted to combine these two aspects of modelling in 2D; in [5] this model was extended to 3D and comparisons made between the two.

We now wish to model the propagation of sound from a duct outlet, in order to inform our choice of radiation condition for the duct itself. Rather than a duct radiating sound into free space, we

[1]freddie.jensen@warwick.ac.uk

[2]E.J.Brambley@warwick.ac.uk (corresponding author)

use a method inspired by Kemp et al. [6] and consider an inner duct positioned within an outer duct, in order to simulate, e.g. the room in which a trumpet is being played. The inner duct is modelled in this context as an acoustic source at arclength $s = 0$ whose width is a fraction $\eta < 1$ of the outer duct width. The right (positive s-facing) side of the source then emanates sound into the outer duct, while the left side will have an acoustic absorption condition to be specified later. This is obviously an idealisation, as the body of the inner duct is not present in the outer domain. However, the expectation is that, for sound leaving the bell of a trumpet: only a small proportion will emanate backwards; a yet smaller proportion will reflect off the body of the trumpet; and this small fraction of reflected sound is unlikely to have a significant influence on the inner duct's acoustics.

2. FORMULATION OF THE GOVERNING EQUATIONS

What follows is a condensed version of the method outlined in Jensen and Brambley [5]. We nondimensionalise the equations of adiabatic gas dynamics, and expand them for small Mach number M, eliminating the density variable when we do so. A duct geometry is introduced: this consists of (i) a centreline with curvature κ, and additionally in 3D torsion τ, and (ii) a width X in 2D and R in 3D. Each of these may vary along the duct, with the arclength variable s. In 2D the wall width may vary either side of the centreline according to functions $X_\pm(s)$, with $X = X_+ - X_-$. The velocity is expressed in a coordinate system moving with the centreline, and its transverse components are eliminated, leaving two acoustic variables: the pressure and the longitudinal velocity.

These two acoustic variables are then subject to two series expansions. Firstly, a Fourier series expansion in time, justified by the fact that musical instruments emit discrete spectra,

$$p'(\mathbf{x},t) = \sum_{a=-\infty}^{\infty} P^a(\mathbf{x}) e^{-ia\omega t}, \qquad u'(\mathbf{x},t) = \sum_{a=-\infty}^{\infty} U^a(\mathbf{x}) e^{-ia\omega t}, \tag{1}$$

where ω is the fundamental frequency and the sum over a represents tonal harmonics. The Fourier coefficients are then projected onto an orthogonal basis of spatial modes, resulting from consideration of the straight-duct problem:

$$P^a(\mathbf{x}) = \sum_{\alpha=0}^{\infty} P^a_\alpha(s)\psi_\alpha(\mathbf{x}), \qquad U^a(\mathbf{x}) = \sum_{\alpha=0}^{\infty} U^a_\alpha(s)\psi_\alpha(\mathbf{x}). \tag{2}$$

We then write the double-coefficients as vectors in the spatial index, resulting in

$$\frac{\mathrm{d}}{\mathrm{d}s}\begin{pmatrix}\boldsymbol{u}^a\\ \boldsymbol{p}^a\end{pmatrix} = \mathsf{L}^a\begin{pmatrix}\boldsymbol{u}^a\\ \boldsymbol{p}^a\end{pmatrix} + \sum_b \mathcal{N}^{ab}\left\langle\begin{pmatrix}\boldsymbol{u}^{a-b}\\ \boldsymbol{p}^{a-b}\end{pmatrix},\begin{pmatrix}\boldsymbol{u}^b\\ \boldsymbol{p}^b\end{pmatrix}\right\rangle. \tag{3}$$

Here the sans-serif quantities L^a are matrices acting on the mode-vectors, while the calligraphic quantities $\mathcal{N}^{ab}$ are analogous third-rank tensors, for which the angle brackets denote a double-contraction operation. For example, in 3D, the matrix L^a is given by

$$\mathsf{L}^a = \begin{pmatrix} -\frac{R'}{R}\mathsf{W} - \tau\mathsf{H} & ia\omega\left[\left(\mathsf{I} - \frac{\Lambda^2}{a^2\omega^2R^2}\right)(\mathsf{I} - \kappa R\mathsf{A}) - \frac{\kappa\widetilde{\mathsf{A}}}{a^2\omega^2R}\right] \\ ia\omega\Big(\mathsf{I} - \kappa R\mathsf{A}\Big) & \frac{R'}{R}\mathsf{W}^T + \tau\mathsf{H}^T \end{pmatrix}, \tag{4}$$

where W, H, A and $\tilde{\mathsf{A}}$ are constant matrices set by the modal basis, and I the identity. These equations are solved by introducing an admittance, which allows for the prescription of a radiation condition. We can then define tensorial *linear and nonlinear admittances* $\mathsf{Y}^a_{\alpha\beta}$ and $\mathcal{Y}^{ab}_{\alpha\beta\gamma}$. These relate the modal coefficients as follows: for pressure P^a_α and velocity U^a_α

$$U^a_\alpha = \sum_{\beta=0}^{\infty} \mathsf{Y}^a_{\alpha\beta}P^a_\beta + \sum_{b=-\infty,b\neq 0,a}^{\infty}\sum_{\beta,\gamma=0}^{\infty} \mathcal{Y}^{ab}_{\alpha\beta\gamma}P^{a-b}_\beta P^b_\gamma, \tag{5}$$

an operation which, suppressing the upper indices on the admittances as well, we write as $\boldsymbol{u} = \mathsf{Y}\boldsymbol{p} + \mathcal{Y}\langle\boldsymbol{u},\boldsymbol{u}\rangle$. Note that these quantities also have inverses $\mathsf{Z} = \mathsf{Y}^{-1}$ and $\mathcal{Z} = -\mathsf{Z}\mathcal{Y}\langle\mathsf{Z},\mathsf{Z}\rangle$.

3. OUTLET RADIATION CONDITION

We derive an outlet radiation condition by considering a much larger straight duct whose centreline is coincident with that of the original duct at the outlet (which we take here to be at $s = 0$). By considering the straight-duct modal basis in the outer duct, we can derive zero-extension and truncation operators F^T and F which map between the two ducts. For $\{\psi^1_\alpha\}^\infty_{\alpha=0}$ being the orthogonal modal basis in the inner duct and $\{\psi^2_\alpha\}^\infty_{\alpha=0}$ being the orthogonal modal basis in the outer, we have

$$\mathsf{F}_{\alpha\beta} = \int_{S_1} \psi^1_\alpha(\mathbf{x})\psi^2_\beta(\mathbf{x})\mathrm{d}S, \tag{6}$$

where S_1 is the cross-section of the inner duct's outlet. Zero-extending the longitudinal velocity u corresponds to a baffle condition on the inner duct, since this implies a hard wall perpendicular to the outlet. Zero-extending the pressure p corresponds to an acoustic dipole, since we expect waves from such a dipole to cancel at the midpoint between their surfaces of radiation. Instead of considering either of these cases, we define *acoustic jump functions* p^* and u^* as

$$u^*(\mathbf{x},t) = u^R(\mathbf{x},t)|_{s=0^+} - u^L(\mathbf{x},t)|_{s=0^-}, \qquad p^*(\mathbf{x},t) = p^R(\mathbf{x},t)|_{s=0^+} - p^L(\mathbf{x},t)|_{s=0^-}, \tag{7}$$

where R and L superscripts indicate that quantity is defined to the *right* or *left* of the duct outlet. Because we expect these quantities to be nonzero only on the outlet surface of the inner duct, we then zero-extend them, rather than the pressure or velocity. This results in relations

$$\boldsymbol{u}^*_2 = \mathsf{F}^T\boldsymbol{u}^*_1, \qquad \boldsymbol{p}^*_2 = \mathsf{F}^T\boldsymbol{p}^*_1. \tag{8}$$

where '2' quantities are modal coefficients in the outer duct and '1' quantities in the inner.

Physically, this represents an infinitely thin sound source in the outer duct, meaning that the outer duct and the inner duct do not coexist in the same space. However, if one assumes that sound reflection from the walls of the inner duct is minimal, this should not drastically change the result of the calculation. Taking the admittance in the outer duct to be positive characteristic (denoted $\mathsf{Y}_2 = \overline{\mathsf{Y}}_2$, and meaning that only forward-propagating or forward-decaying waves are allowed), and defining quantities $\mathsf{Q} := \left(\mathsf{I} + \mathsf{F}\overline{\mathsf{Y}}_2\mathsf{F}^T\mathsf{Z}^L_1\right)^{-1}$ and $\widetilde{\mathsf{Q}} := \left(\mathsf{I} + \mathsf{Y}^L_1\mathsf{F}\overline{\mathsf{Z}}_2\mathsf{F}^T\right)^{-1}$, we can then derive a relation between the admittance to the left of the outlet Y^L_1, and that to the right, Y^R_1

$$\mathsf{Y}^R_1 = -\left[\mathsf{I} - \widetilde{\mathsf{Q}}^{-1}(\mathsf{I}+\mathsf{Q})\right]^{-1}\left[\mathsf{I} + \widetilde{\mathsf{Q}}^{-1}(\mathsf{I}-\mathsf{Q})\right]\mathsf{Y}^L_1, \tag{9}$$

with a corresponding nonlinear relation

$$\begin{aligned}
\mathcal{Y}^R_1 = \left[\mathsf{I} - \widetilde{\mathsf{Q}}^{-1}(\mathsf{I}+\mathsf{Q})\right]^{-1}\Bigg\{ &\left[\mathsf{I} - \widetilde{\mathsf{Q}}^{-1}(\mathsf{I}-\mathsf{Q})\right]\mathcal{Y}^L_1\left\langle \mathsf{I} - \mathsf{Z}^L_1\mathsf{Q}\left(\mathsf{Y}^L_1 + \mathsf{Y}^R_1\right), \cdots\right\rangle \\
-\frac{1}{4}&\left(\mathsf{Y}^L_1\mathsf{F}\overline{\mathsf{Z}}_2 - \widetilde{\mathsf{Q}}^{-1}\mathsf{Q}\mathsf{F}\right)\overline{\mathcal{Y}}_2\left\langle \mathsf{F}^T\mathsf{Z}^L_1\mathsf{Q}\left(\mathsf{Y}^L_1 + \mathsf{Y}^R_1\right) - \overline{\mathsf{Z}}_2\mathsf{F}^T\left[(\mathsf{I}+\mathsf{Q})\mathsf{Y}^R_1 - (\mathsf{I}-\mathsf{Q})\mathsf{Y}^L_1\right], \cdots\right\rangle \\
-\frac{1}{4}&\left(\mathsf{Y}^L_1\mathsf{F}\overline{\mathsf{Z}}_2 + \widetilde{\mathsf{Q}}^{-1}\mathsf{Q}\mathsf{F}\right)\overline{\mathcal{Y}}_2\left\langle \mathsf{F}^T\mathsf{Z}^L_1\mathsf{Q}\left(\mathsf{Y}^L_1 + \mathsf{Y}^R_1\right) + \overline{\mathsf{Z}}_2\mathsf{F}^T\left[(\mathsf{I}+\mathsf{Q})\mathsf{Y}^R_1 - (\mathsf{I}-\mathsf{Q})\mathsf{Y}^L_1\right], \cdots\right\rangle\Bigg\}.
\end{aligned} \tag{10}$$

Since the left-hand surface of the sound source should not be accessible by sound emitting from the right-hand surface (since physically this would correspond to sound from a trumpet finding its way back inside the bell from the side) we make up for this problem by taking the left-hand side's admittances to be those of a perfectly absorbing duct, i.e. $\mathsf{Y}^L_1 = \overline{\mathsf{Y}}_1$ and $\mathcal{Y}^L_1 = \overline{\mathcal{Y}}_1$. Thus, in terms of the two ducts' characteristic admittances, and the zero-extension and truncation operators, we have an outlet condition.

4. SOLUTION OF THE GOVERNING EQUATIONS

There are three steps to solving for the acoustic field in the full domain (consisting of both the inner and outer ducts). We set the admittance at the outlet of the inner duct, and solve a Riccati-style equation for the admittance backwards to its inlet, with coefficients set by the duct geometry (step 1). This Riccati equation is derived by substituting the definition of the admittance (5) into the governing equations (3) and cancelling off the pressure; for more detail see Jensen and Brambley [5]. Once solved, we know the radiative properties of the duct, so we prescribe a pressure condition at the inlet (generally either a piston or specifying the forward-travelling component only). This is then substituted into the lower block of equation (3) and solved forwards towards the outlet (step 2). We can derive conditions to relate the inner-duct outlet pressure $\boldsymbol{p}_1^R$ to the outer-duct pressures at that point $\boldsymbol{p}_2^R$ and $\boldsymbol{p}_2^L$, and solve in the outer duct forwards and backwards from there respectively (step 3).

We may neglect certain of these steps at various points. If we only wish to know the pressure in the inner duct given the outer duct's presence, we can neglect step 3; alternatively we can model the inner duct as an $n-1$-dimensional source (in n dimensions) and ignore its internal acoustics entirely (this is neglect of steps 1 and 2). We are also interested in the impedance at the inlet, which can be calculated using only step 1; meanwhile for calculation of the end correction coefficients, we may neglect all three steps. The last two cases are explored for a range of frequencies, so it is fortunate that they can be completed in much less time and using much less computational power.

5. NUMERICAL METHOD

5.1. Truncation

When solving this set of countably infinite temporally and spatially-coupled ODEs, we must truncate the number of modes in each direction. Thinking carefully about symmetries we can exploit, we find that there are $(\alpha_{\max}+1)a_{\max}$ independent equations for P^a_α, $(\alpha_{\max}+1)^2 a_{\max}$ for $\mathsf{Y}^a_{\alpha\beta}$, and $3(\alpha_{\max}+1)^3 a_{\max}(a_{\max}-1)/2$ for $\mathcal{Y}^{ab}_{\alpha\beta\gamma}$. Here $\alpha_{\max}$ refers to the number of spatial modes for whatever domain in which the acoustic pressure is currently being calculated. In general we follow the rule of thumb set by McTavish [7] that $\alpha^2_{\max} \geq \alpha^1_{\max}/\eta$, where $\eta < 1$ is the size comparison factor.

5.2. Numerical Viscosity

One of the pitfalls of truncation is the pooling of energy at higher modes. This can be counteracted by employing a numerical viscosity. Numerical viscosity is derived by considering the truncation error of a sawtooth wave when substituted into the governing equations. The sawtooth wave as derived by Fay [8] has Fourier coefficients given by

$$P^a = \frac{iMe^{ia\omega s}}{a(1+\sigma)} \tag{11}$$

where $\sigma = \beta_0 M\omega s$ is the arclength normalised by shock-formation distance. The truncation error of the nonlinear term is then

$$E^a = -\frac{i\omega\beta_0\sqrt{A_{\mathrm{cs}}}M^2 e^{ia\omega s}}{1+\sigma^2}\left(\sum_{\substack{b=-\infty,\\ b\neq 0,a}}^{\infty} - \sum_{\substack{b=a-\mathrm{sgn}(a)a_{\max},\\ b\neq 0,a}}^{\mathrm{sgn}(a)a_{\max}}\right)\frac{a}{2(a-b)b}. \tag{12}$$

This can be approximated as

$$E^a \approx -\frac{|a|\omega\beta_0 M P^a_0}{1+\sigma}\log\left(1-\frac{|a|-1}{a_{\max}}\right) \sim \frac{|a|^2\omega\beta_0 M P^a_0}{a_{\max}} \tag{13}$$

where the second approximation here is in the limit of small distances, and with $1 \ll |a| \ll a_{\max}$ (where energy pooling starts to occur). We subtract this term from our equations, where it acts as a numerical viscosity.

6. RESULTS

6.1. Prediction of the end-correction coefficient

We are interested in a linear acoustic extension of the 'end correction' problem. For plane waves, the end correction may be defined for a pressure field

$$p' = A\left(e^{ikx-i\omega t} + |R|e^{-ikx-i\omega t+i\arg(R)}\right), \tag{14}$$

with $k \in \mathbb{R}$. A node in the pressure is closest to occurring at some $x_{\mathrm{ec}} > x_{\mathrm{o}}$ where the incident and reflected waves are out of phase, giving

$$x_{\mathrm{ec}} = \frac{\arg(R) \pm \pi}{2k}, \tag{15}$$

while $|R|$ is unconstrained. If k is imaginary, the phase cannot be constrained in the same way, so the end correction is only defined for cut-on modes.

Attempting to generalise this, we express the pressure in terms of the ansatz solutions for the straight duct problem

$$P^a(\mathbf{x}) = \sum_\alpha \psi_\alpha(\mathbf{x})\left(e^{\overline{\gamma}^a_\alpha s}A^{a+}_\alpha + e^{-\overline{\gamma}^a_\alpha s}\sum_\beta \mathsf{R}^a_{\alpha\beta}A^{a+}_\beta e^{(\overline{\gamma}^a_\alpha+\overline{\gamma}^a_\beta)s_{\mathrm{o}}}\right) = \sum_{\alpha,\beta}\psi_\alpha(\mathbf{x})\left(e^{\overline{\gamma}^a_\alpha \hat{s}}\delta_{\alpha\beta} + \mathsf{R}^a_{\alpha\beta}e^{-\overline{\gamma}^a_\alpha \hat{s}}\right)A^{a+}_\beta e^{\overline{\gamma}^a_\beta s_{\mathrm{o}}}. \tag{16}$$

where $\hat{s} = s - s_{\mathrm{o}}$. Since we do not have a sensible definition of the end correction for cut-off waves, we restrict ourselves to the case of both waves being cut-on. Further to this, because we are comparing the arguments of entries in the reflection matrix to those of the matrix $e^{\overline{\gamma}^a_\alpha \hat{s}}\delta_{\alpha\beta}$, which is diagonal, we correspondingly only consider the reflection matrix's diagonal entries. This results in a vector of end corrections $\hat{s}^a_\alpha$, where each entry is given by

$$\hat{s}^a_\alpha = \begin{cases} \frac{\arg \mathsf{R}^a_{\alpha\alpha}+\pi}{2\,\mathrm{Im}(\overline{\gamma}^a_\alpha)}, & \mathrm{Im}(\overline{\gamma}^a_\alpha) \neq 0, \\ 0, & \mathrm{Im}(\overline{\gamma}^a_\alpha) = 0. \end{cases} \tag{17}$$

The reflection matrix can be calculated using the outlet admittance condition.

Figure 1 plots the end correction for various modes as a function of the Helmholtz number ωX for a two-dimensional duct. In contrast to the well-known low-frequency end correction of $\hat{s}^1_0 \approx 0.6$ for three-dimensional ducts, in two dimensions the end correction exhibits a logarithmic singularity at low frequencies. Moreover, the end correction exhibits a cusp every time an new duct mode cuts on. An analytic solution can also be found for the end correction using the Wiener–Hopf method [9]. The Wiener–Hopf solution is also plotted in figure 1, and demonstrates the same behaviour.

6.2. Resonances in a finite-length duct

There are multiple ways to calculate the resonances in a duct of finite length. One method is to consider the impedance at the duct inlet. Physical instruments can have either one or two openings (described as 'closed' or 'open' ducts respectively). If the duct is 'closed', we expect a minimum in the velocity at the inlet, corresponding to a very high impedance. Conversely, if it is open, the free-space condition at the inlet will result in a pressure minimum, i.e. a low impedance. Defining a scalar impedance as

$$|Z| = \sqrt{\frac{\sum_{a=-\infty}^{\infty}\sum_{\alpha=0}^{\infty}|P^a_\alpha|^2}{\sum_{a=-\infty}^{\infty}\sum_{\alpha=0}^{\infty}|U^a_\alpha|^2}}, \tag{18}$$

and calculating it at the inlet for a range of frequencies, we can deduce information about the tone and harmonic series of the duct in question.

In figure 2, these calculations are performed for 3D ducts of varying aspect ratio. The

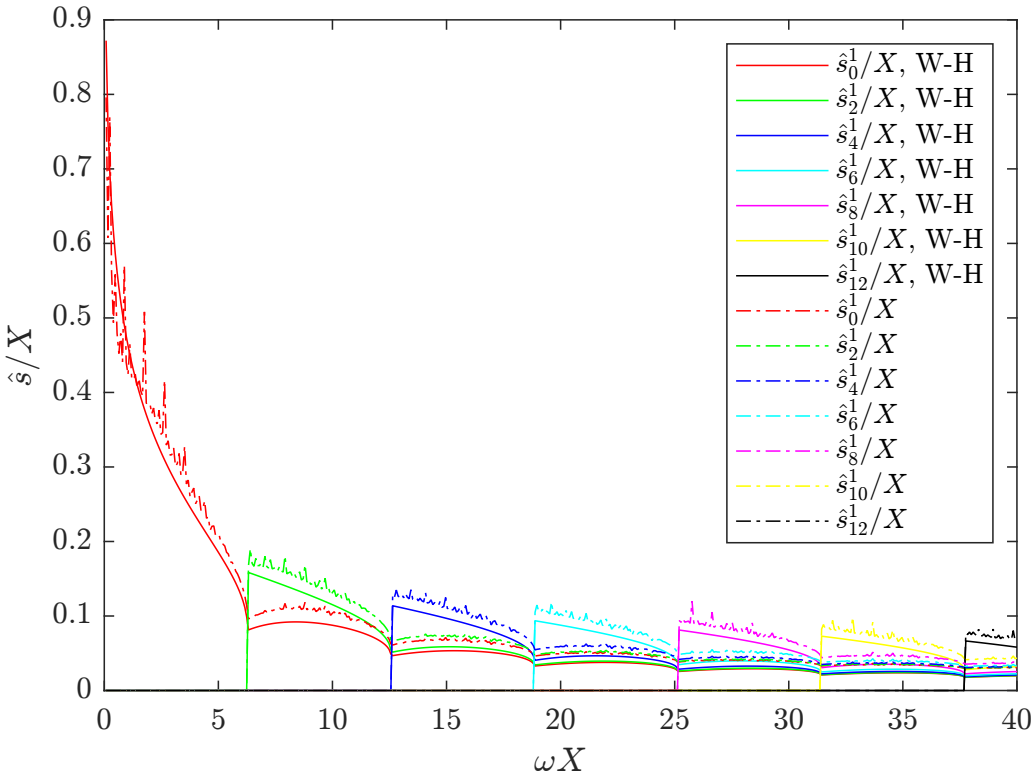

Figure 1: End-correction coefficients for a two-dimensional duct, calculated using the Wiener-Hopf method (solid line) and using our outlet condition (dash-dotted line).

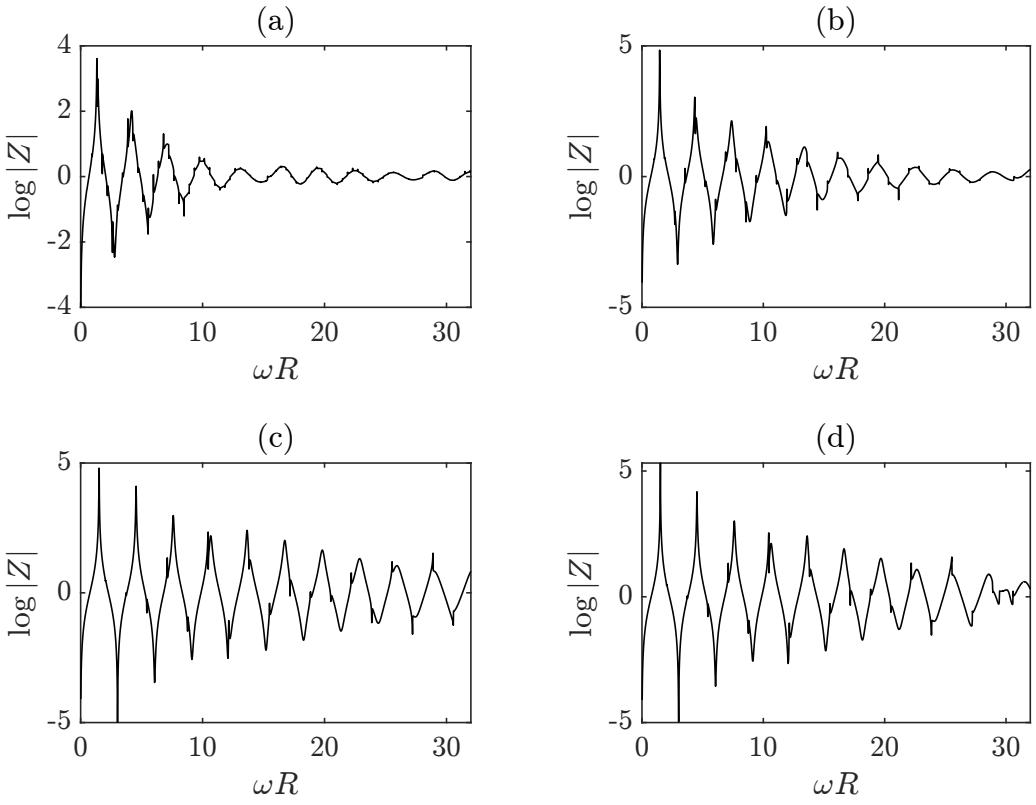

Figure 2: Inlet impedance plots for a range of frequencies in 3D, for (a) a straight duct of aspect ratio 1/4; (b) a straight duct of aspect ratio 1/8; (c) a straight duct of aspect ratio 1/16; and (d) a curved duct of aspect ratio 1/16. Maxima represent the resonances of a closed duct, while minima represent those of an open duct. For 'longer' ducts, the higher harmonics have more pronounced resonances, while for 'shorter' ducts the higher harmonics are more suppressed.

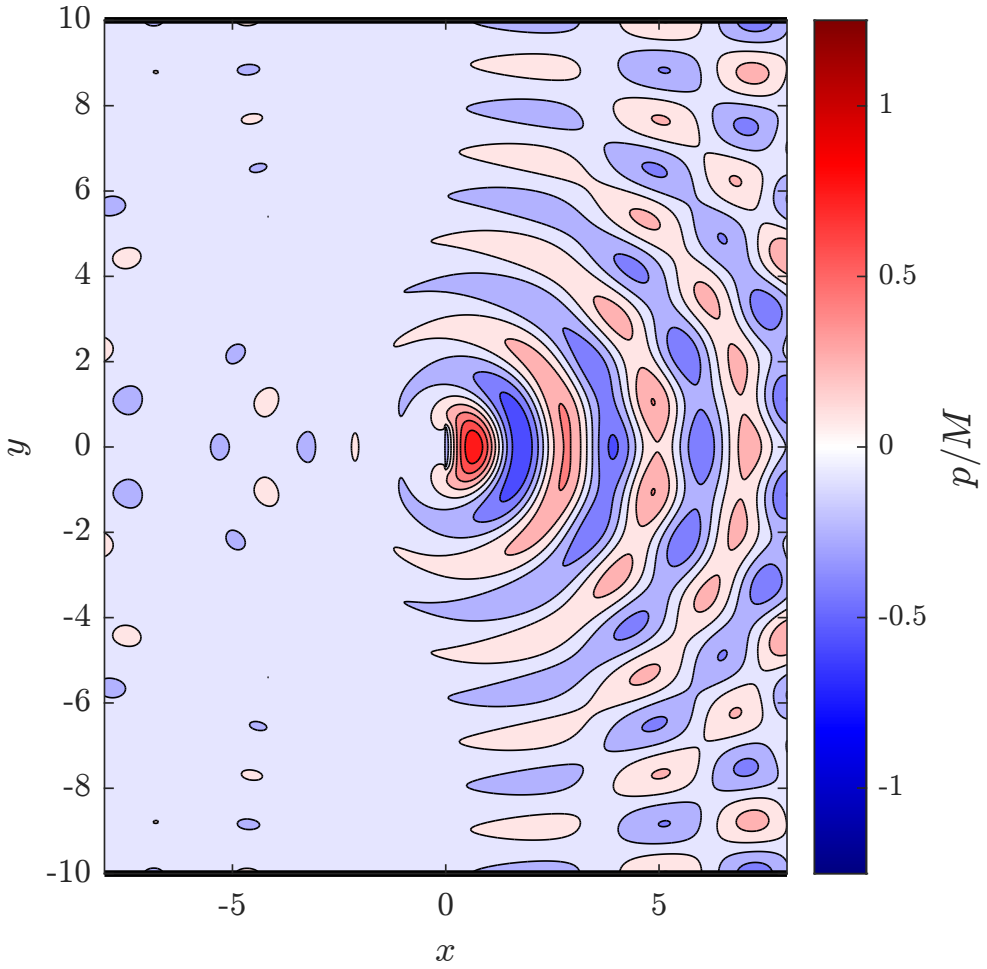

Figure 3: Acoustic field emanating from a one-dimensional acoustic source into a two-dimensional duct 20 times larger. 10 modes were used in the inner calculation and 200 modes in the outer, with $\omega X_1 = 3$ for X_1 the inner width.

maxima occur (roughly) at odd-integer frequency multiples of the first maximum (or *closed-duct fundamental*), consistent with the harmonic series of a 'closed' instrument (the boundary conditions on such instruments admit oscillations of a quarter-wavelength and all odd multiples thereof). The minima, meanwhile, occur (roughly) at integer multiples of the first minimum (or *open-duct fundamental)*, consistent with the harmonic series of an 'open' instrument (whose boundary conditions admit integer multiples of a half-wavelength).

Also notable are the variations in the magnitude of the maxima/minima across different aspect ratios. More pronounced maxima/minima occur for more extreme aspect ratios; this agrees with the fact that broad organ pipes have a tone much more fundamental-dominated than slender ones. Between plots (c) and (d) in figure 2 we are able to assess the difference that a bent duct makes: up to the eighth peak very little changes, but from that point the bent duct behaves differently, in particular with a split resonance after the ninth peak.

6.3. Linear radiation from an acoustic source

We can calculate the acoustic field in the outer duct without considering the inner duct's acoustics: this is achieved by modelling the inner duct as an $(n-1)$-dimensional sound source emitting plane waves in one direction and absorbing waves from the other. The pressure field due to such a source is plotted in figure 3. We see that the absorbing boundary condition on the 'backplate' surface has resulted in radiation travelling predominantly rightward from the outlet: this suggests that the absorbing condition is a reasonable workaround for the problem of the intersecting inner-duct

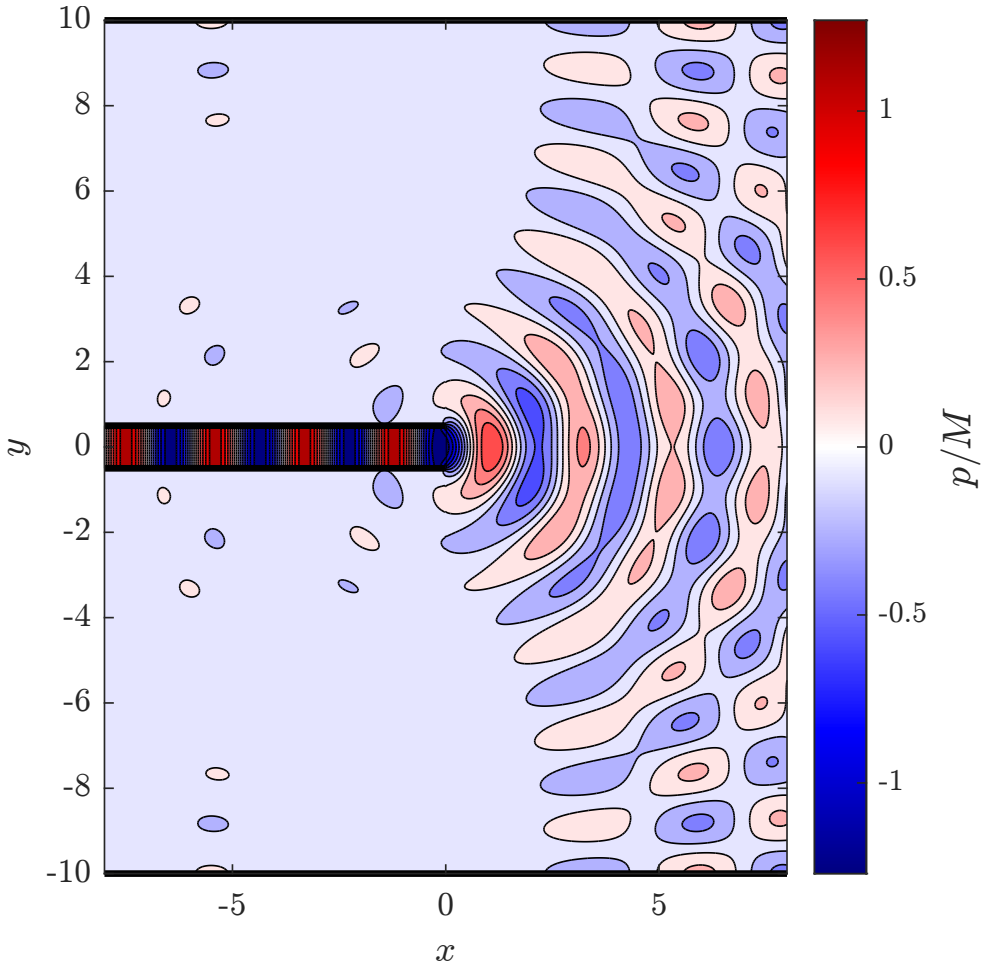

Figure 4: Acoustic field emanating from a straight duct into a duct 20 times larger, in two dimensions. 10 modes were used in the inner calculation and 200 modes in the outer, with $\omega X_1 = 3$ for X_1 the inner width.

and outer-duct geometries.

6.4. Linear radiation from a straight duct

In contrast to the previous section, we can also choose to calculate the inner-duct acoustic field to see how sound exits from the outlet. This is done in two dimensions in figure 4, and in three dimensions in figure 5. Comparing the 2D duct (figure 4) with a 2D source (figure 3), we unsurprisingly see great similarity, with any differences between the contours being attributable to a phase difference due to the duct length not being a multiple of the wavelength. Comparing the 2D duct (figure 4) with the 3D duct (figure 5), it is clear that compared with the duct interior, the radiation from the outlet in 3D has a much lower amplitude than in 2D, as the decay rate in 3D is $1/r$ with distance from the exit while it is $1/\sqrt{r}$ in 2D. However, the acoustics within the inner ducts appear to behave similarly between the two cases.

6.5. Nonlinear acoustics within an open straight duct

We can also calculate the acoustic field within a straight duct in the nonlinear regime, shown in the 2D case in figure 6 for a perturbation Mach number of $M = 0.1$. Extending this calculation to the outer duct is computationally costly, due to the vastly greater number of spatial modes required, but we can still apply the radiation condition and see what effect it has on the acoustics within the inner duct. An immediately noticeable physical effect that is not achieved with the idealised boundary condition

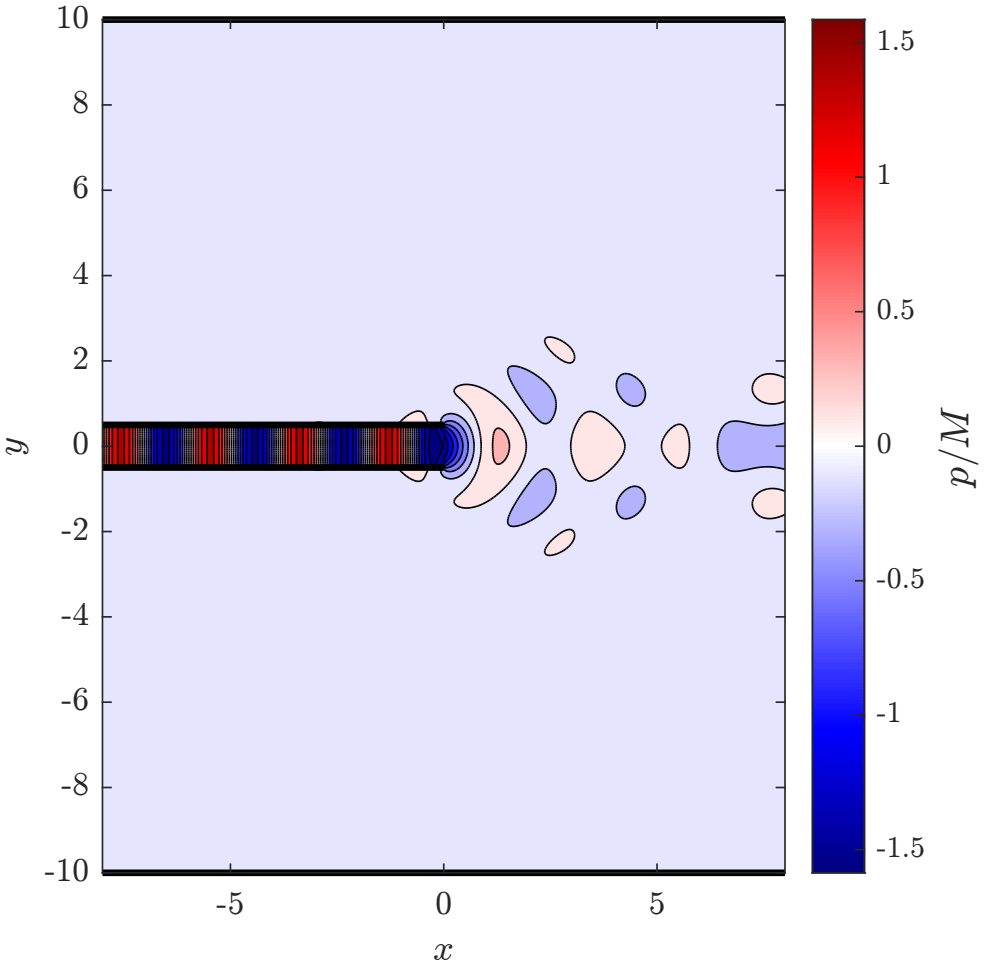

Figure 5: Acoustic field emanating from a straight duct into a duct 20 times larger, in three dimensions. 10 modes were used in the inner calculation and 200 modes in the outer, with $\omega R_1 = 3/2$ for R_1 the inner radius.

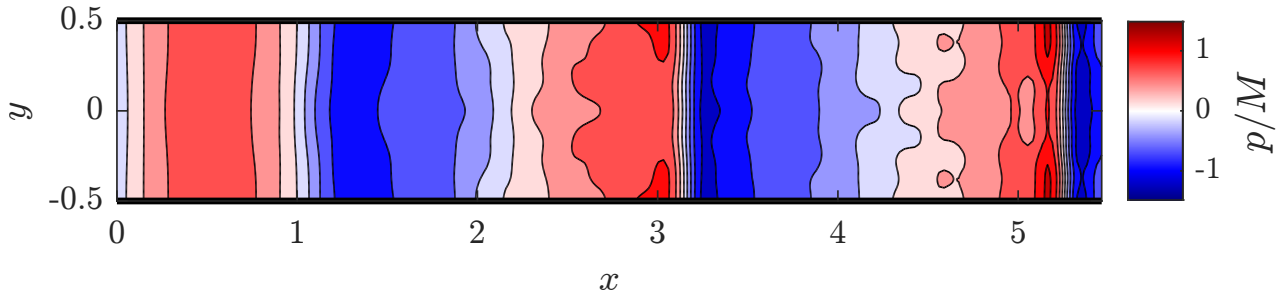

Figure 6: Nonlinear acoustic field within a straight duct opening into a duct 20 times larger, in two dimensions. 10 modes were used in the inner calculation and 200 modes in the outer, with $\omega X_1 = 3$ for X_1 the inner radius. The perturbation Mach number is $M = 0.1$.

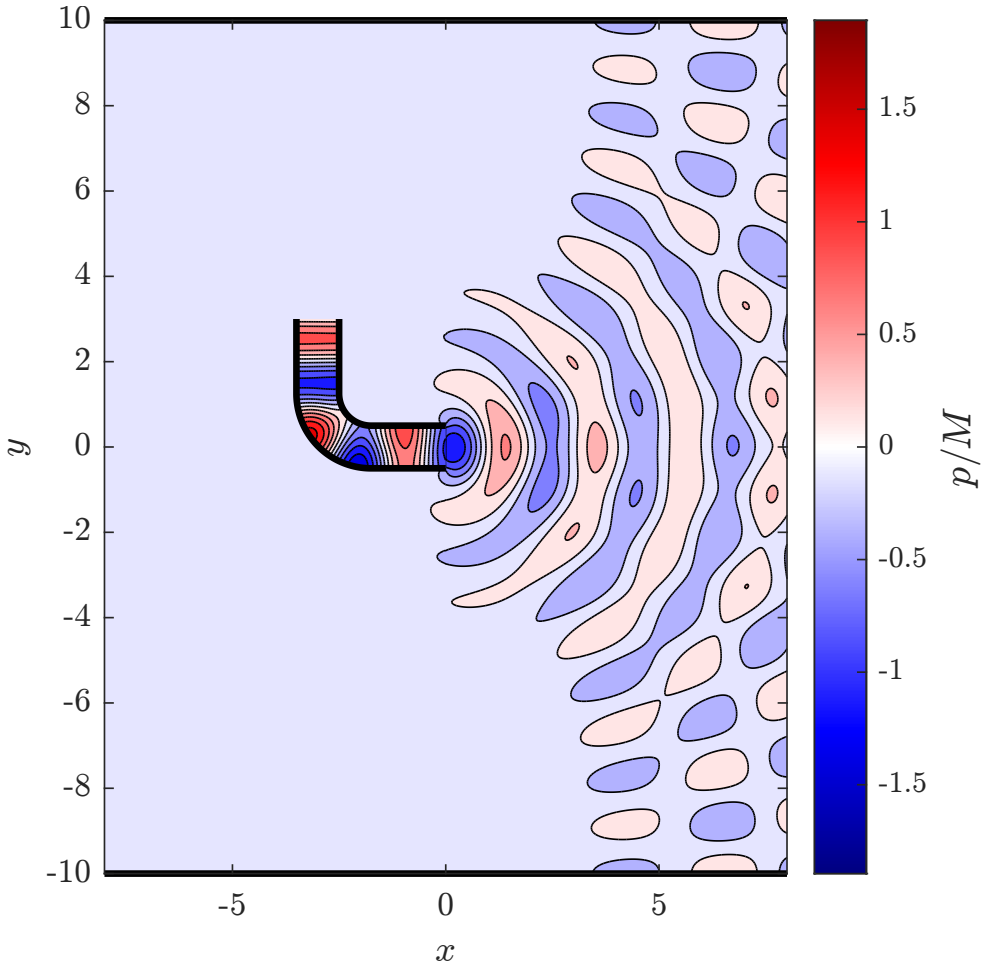

Figure 7: Acoustic field emanating from a curved duct into a duct 20 times larger, in two dimensions. 10 modes were used in the inner calculation and 200 modes in the outer, with $\omega X_1 = 3$ for X_1 the inner radius.

from Jensen and Brambley [5] is that non-plane waves are excited: this is due to the geometry of the outlet, and nonlinear reflections back from it. In the linear case, the non-plane reflections are not observable, as in figure 4, but here they are very clearly visible.

6.6. Linear radiation from a curved duct

The final case we consider is that radiation from a duct with a curved section into a larger straight duct, in two dimensions, shown in figure 7. We can see that despite the asymmetry of the source, the radiation from the end is almost symmetric across the midline. Since symmetric and antisymmetric waves are completely uncoupled in the outer duct, this suggests that the radiation from the inner duct is predominantly symmetric.

7. CONCLUSIONS

We have presented current progress made in applying a more physically realistic outlet condition to the existing model of nonlinear curved-duct acoustics [5]. Presented is a strong theoretical model, together with a growing computational framework with which to apply it, involving both direct solution of the acoustic field and measurement of physically important parameters such as the end correction factor and the inlet impedance.

Future work will attempt to further investigate the nonlinear regime. For example, knowing how the resonances' locations change with amplitude will be informative as to the relationship between

volume and tone of a brass instrument. Also worthy of study is how the end-correction coefficient varies with Mach number. Moreover, an analytic treatment of the 3D case is currently in progress, and reproducing the well-known plane-wave result of $\hat{s}/X \approx 0.6$, working towards quantifying how this varies with aspect ratio and Mach number.

Another direction of future work would be to address the problem of the outer and inner ducts' domain intersection. Given a modal basis for an outer duct of annular cross-section, the zero-extension and truncation operators between this and the inner-duct modes could be used to derive a more realistic outlet condition for a straight duct. The model would be less versatile for non-straight inner ducts, but would at least facilitate a comparison with the current work to assess the impact of externally reflected waves.

ACKNOWLEDGMENTS

FJ is carrying out this work as a participant in the Warwick Doctoral Training Programme (DTP), and EJB is grateful for the support of EPSRC grant (EP/V002929/1).

REFERENCES

1. Hirschberg, Gilbert, Msallam, and Wijnands, (1996). "Shock waves in trombones". *J. Acoust. Soc. Am*, **99** 1754–1758. doi: 10.1121/1.414698.
2. Fernando and Druon, (2011). "Nonlinear waves and shocks in a rigid acoustical guide". *J. Acoust. Soc. Am*, **129** 604–615. doi: 10.1121/1.3531799.
3. Félix and Pagneux, (2002). "Multimodal analysis of acoustic propagation in three-dimensional bends". *Wave Motion*, **36** 157–168. doi: 10.1016/S0165-2125(02)00009-4.
4. McTavish and Brambley, (2019). "Nonlinear sound propagation in two-dimensional curved ducts: A multimodal approach". *J. Fluid Mech*, **875** 411–447. doi: 10.1017/jfm.2019.497.
5. Jensen and Brambley. "Multimodal nonlinear acoustics in two- and three-dimensional curved ducts", (2025). https://arxiv.org/abs/2503.11536. (submitted to J. Fluid Mech.).
6. Kemp, Lopez-Carromero, and Campbell, (2017). "Pressure fields in the vicinity of brass musical instrument bells measured using a two dimensional grid array and comparison with multimodal models". In *Proceedings of the 24th International Congress on Sound and Vibration*. https://hdl.handle.net/10023/12128.
7. McTavish, (2018). *Nonlinear acoustics in a general waveguide*. PhD thesis, University of Cambridge. doi: 10.17863/CAM.35714.
8. Fay, (1931). "Plane sound waves of finite amplitude". *J. Acoust. Soc. Am*, **3** 222–241. doi: 10.1121/1.1915557.
9. Noble, (1958). *Methods based on the Wiener–Hopf Technique for the Solution of Partial Differential Equations*. Pergamon. ISBN 0828403325.